

PAPER

# Excellent ethanol sensing properties based on $\text{Er}_2\text{O}_3\text{-Fe}_2\text{O}_3$ nanotubes

To cite this article: Chang-Bai Liu *et al* 2015 *Chinese Phys. B* **24** 118501

View the [article online](#) for updates and enhancements.

## You may also like

- [High Performance Metal-Insulator-Metal Capacitors with  \$\text{Er}\_2\text{O}\_3\$  on ALD  \$\text{SiO}\_2\$  for RF Applications](#)  
Thanh Hoa Phung, Dharani Kumar Srinivasan, Philipp Steinmann et al.
- [Structural and Optical Properties of Nanocrystalline  \$\text{Er}\_2\text{O}\_3\$  Thin Films Deposited by a Versatile Low-Pressure MOCVD Approach](#)  
Maria Losurdo, Maria M. Giangregorio, Pio Capezzuto et al.
- [Synthesis, characterization, and photoluminescence of  \$\text{Er}\_2\text{O}\_3\text{-Er}\_2\text{SO}\_4\$  nanoparticles on reduced graphene oxide](#)  
Nikolai G Kalugin, Aaron J Roy, Kateryna Artyushkova et al.

# Excellent ethanol sensing properties based on $\text{Er}_2\text{O}_3\text{-Fe}_2\text{O}_3$ nanotubes\*

Liu Chang-Bai(刘唱白)<sup>a)†</sup>, He Ying(何 滢)<sup>b)</sup>, and Wang Sheng-Lei(王圣蕾)<sup>a)</sup>

<sup>a)</sup> College of Electronic Science & Engineering, Jilin University, Changchun 130012, China

<sup>b)</sup> College of Instrumentation & Electrical Engineering, Jilin University, Changchun 130012, China

(Received 9 April 2015; revised manuscript received 19 June 2015; published online 10 October 2015)

In this work, pure  $\alpha\text{-Fe}_2\text{O}_3$  and  $\text{Er}_2\text{O}_3\text{-Fe}_2\text{O}_3$  nanotubes were synthesized by a simple single-capillary electrospinning technology followed by calcination treatment. The morphologies and crystal structures of the as-prepared samples were characterized by scanning electron microscopy and x-ray diffraction, respectively. The gas-sensing properties of the as-prepared samples have been researched, and the result shows that the  $\text{Er}_2\text{O}_3\text{-Fe}_2\text{O}_3$  nanotubes exhibit much better sensitivity to ethanol. The response value of  $\text{Er}_2\text{O}_3\text{-Fe}_2\text{O}_3$  nanotubes to 10 ppm ethanol is 21 at the operating temperature  $240^\circ$ , which is 14 times larger than that of pure  $\alpha\text{-Fe}_2\text{O}_3$  nanotubes (response value is 1.5). The ethanol sensing properties of  $\alpha\text{-Fe}_2\text{O}_3$  nanotubes are remarkably enhanced by doping Er, and the lowest detection limit of  $\text{Er}_2\text{O}_3\text{-Fe}_2\text{O}_3$  nanotubes is 300 ppb, to which the response value is about 2. The response and recovery times are about 4 s and 70 s to 10 ppm ethanol, respectively. In addition, the  $\text{Er}_2\text{O}_3\text{-Fe}_2\text{O}_3$  nanotubes possess good selectivity and long-term stability.

**Keywords:**  $\text{Er}_2\text{O}_3$ ,  $\alpha\text{-Fe}_2\text{O}_3$  nanotubes, ethanol, gas sensing

**PACS:** 85.85.+j, 85.35.-p, 81.07.-b

**DOI:** 10.1088/1674-1056/24/11/118501

## 1. Introduction

Semiconductor oxides have been widely studied, due to their applications in lithium storage,<sup>[1,2]</sup> photosensitization,<sup>[3,4]</sup> and gas sensors.<sup>[5-7]</sup> In particular, in the fields of gas sensors, the semiconductor oxides play an important role. It is necessary to detect the inflammable, explosive and toxic gases in our daily lives to maintain safety, such as hydrogen,<sup>[8]</sup> carbonic oxide,<sup>[9]</sup> and ethanol.<sup>[10]</sup> Ethanol is an important gas which is widely used in our lives, such as in the fields of industry, medicophysics, and food production. In addition, ethanol is an inflammable, explosive, and toxic gas. Therefore, it is necessary to make an ethanol gas sensor to monitor it in order to avoid danger. In recent years, various kinds of semiconductor oxide ethanol sensors have been made, such as  $\text{ZnO}$ ,<sup>[11]</sup>  $\text{SnO}_2$ ,<sup>[12]</sup>  $\text{In}_2\text{O}_3$ ,<sup>[13]</sup> and  $\text{Fe}_2\text{O}_3$ <sup>[14]</sup> sensors. However, the present works have demonstrated that there are some disadvantages of pure semiconductor oxides for using in gas sensors, such as low sensibility and poor selectivity. Therefore, many works have been done to solve these problems. At present, the most simple and effective way is doping other elements. The gas-sensing properties of electrospun  $\text{In}_2\text{O}_3$  nanotubes are improved by doping Mg.<sup>[15]</sup> Doping Sr will enhance discriminative ability from acetone of  $\text{SnO}_2$  nanofibers ethanol chemiresistor.<sup>[16]</sup>

Among the common semiconductor oxides, hematite ( $\alpha\text{-Fe}_2\text{O}_3$ ) has been attracting more and more attention in recent years, due to the fact that it is a stable, low-cost, non-

toxic, and easy available compound, which is profitable in gas sensors. In recent years, various one-dimensional (1D)  $\alpha\text{-Fe}_2\text{O}_3$  nanostructures have been synthesized for gas sensors, such as nanoparticles,<sup>[17]</sup> nanobelts,<sup>[18]</sup> nanorods,<sup>[19]</sup> and nanotubes.<sup>[20]</sup> Many works have proved that the exposure of the inner/outer surfaces of nanotubes will provide larger reactive sites, which is beneficial to gas sensing.<sup>[21,22]</sup> However, pure  $\alpha\text{-Fe}_2\text{O}_3$  shows poor sensibility. Thus, many efforts have been done to improve the sensibility of pure  $\alpha\text{-Fe}_2\text{O}_3$  and the most simple and efficient way is doping. Cu is used as the dopant for improving the gas sensing properties of  $\alpha\text{-Fe}_2\text{O}_3$  hierarchical microcubes.<sup>[23]</sup>  $\text{Au}/\alpha\text{-Fe}_2\text{O}_3$  shows much better sensitive to acetone than  $\alpha\text{-Fe}_2\text{O}_3$ .<sup>[24]</sup> Rare earth elements have been extensively studied over the past decades due to their particular characteristics.<sup>[25,26]</sup> The gas-sensing properties of materials have been enhanced by the mean of doping rare earth elements which is proved by the previous works.<sup>[27-30]</sup> Hence, as one of the rare earth elements, Er is used for enhancing the gas sensing properties of materials.<sup>[31,32]</sup> However, there are few works to study the effect on the sensing properties of  $\alpha\text{-Fe}_2\text{O}_3$  nanotubes by doping Er. In this paper, pure  $\alpha\text{-Fe}_2\text{O}_3$  and  $\text{Er}_2\text{O}_3\text{-Fe}_2\text{O}_3$  nanotubes are successfully synthesized via the single nozzle electrospinning and calcination method. The results of the sensing research show that the ethanol sensing properties of pure  $\alpha\text{-Fe}_2\text{O}_3$  nanotubes is enhanced remarkably by doping Er. Moreover, the  $\text{Er}_2\text{O}_3\text{-Fe}_2\text{O}_3$  nanotube sensors show a fast response time, good selectivity, and long-term stability.

\*Project supported by Jilin Provincial Science and Technology Department, China (Grant No. 20140204027GX) and the Challenge Cup for College Students, China (Grant No. 450060497053).

†Corresponding author. E-mail: liwei99@jlu.edu.cn

## 2. Experimental

### 2.1. Materials

All the chemistry reagents were analytical grade and used without further purification. Poly (vinyl pyrrolidone) (PVP, Mw = 1300000) was obtained from Sigma-Aldrich (USA).  $\text{Fe}(\text{NO}_3)_3 \cdot 9\text{H}_2\text{O}$  (99.99%),  $\text{Er}(\text{NO}_3)_3 \cdot 6\text{H}_2\text{O}$  (99.99%), N,N-dimethylformamide (DMF,  $\geq 99.5\%$ ) and ethanol ( $\geq 99.7\%$ ) were purchased from Aladdin (China).

### 2.2. Synthesis of pure $\alpha\text{-Fe}_2\text{O}_3$ and $\text{Er}_2\text{O}_3\text{-Fe}_2\text{O}_3$ nanotubes

At first, 0.55-g PVP was mixed with 5.9-g ethanol. Meanwhile, 1.9-g DMF was mixed with 0.49-g  $\text{Fe}(\text{NO}_3)_3 \cdot 9\text{H}_2\text{O}$  and an amount of  $\text{Er}(\text{NO}_3)_3 \cdot 6\text{H}_2\text{O}$  (in a weight ratio of 0%, 1 wt%, 3 wt%, and 5 wt%). Then, the two mixtures were stirred for 1 h. At last, the two mixtures were mixed and stirred for 12 h. Then, the precursor solution was prepared. The precursor solution was jetted from a single stainless steel capillary. The non-woven mats collector was about 20 cm away from the capillary, and the voltage value was 13 kV. Subsequently, the collected composite fibers were calcined at 550 °C for 4 h with the heating rate of 15 °C/min and natural cooling to obtain the pure  $\alpha\text{-Fe}_2\text{O}_3$  and  $\text{Er}_2\text{O}_3\text{-Fe}_2\text{O}_3$  nanotubes.

### 2.3. Fabrication of gas sensor

The process of gas sensor fabrication is described in the previous work.<sup>[33]</sup> In detail, an amount of deionized water was mixed with the samples to form slurry. Subsequently, a ceramic tube was coated with the slurry on which there is a pair of gold electrodes. A spring-like Ni-Cr was used to provide operating temperature which was plugged into the ceramic tube. The gas sensors need to be dried for three days before the first measurement. The sensor response ( $S = R_a/R_g$ ) was defined as the ratio of the sensor resistances in the air ( $R_a$ ) and in the target gas ( $R_g$ ). The time taken by the sensor to achieve 90% of the resistance variation was response time, and when the sensor was opened to the air the time taken to return 90% of the resistance variation was recovery time.

### 2.4. Characterization

The XRD-6000 x-ray diffractometer (XRD, SHIMADZU, Japan) with Cu  $K\alpha 1$  radiation ( $\lambda = 1.5406 \text{ \AA}$ ) was employed to analyze structure characterization. Scanning electron microscope (SEM) images were performed on an FEI XL30 instrument with an energy-dispersive spectrometer (EDS). The sensing properties of the sensor were measured by a CGS-8 intelligent gas-sensing analysis system (Beijing Elite Tech Co., Ltd., China).

## 3. Results and discussion

### 3.1. Structure and morphological characteristics

The nanostructures of the pure  $\alpha\text{-Fe}_2\text{O}_3$  and 3 wt%  $\text{Er}_2\text{O}_3\text{-Fe}_2\text{O}_3$  were investigated by SEM and are shown in Fig. 1. It can be seen that the pure  $\alpha\text{-Fe}_2\text{O}_3$  materials possess the nanotube structure with an average diameter of about 80 nm from Figs. 1(a) and 1(b), and the nanostructure and diameter are basically unchanged after doping Er which is evidenced in Figs. 1(c) and 1(d). TEM images of pure  $\alpha\text{-Fe}_2\text{O}_3$  nanotubes and 3 wt%  $\text{Er}_2\text{O}_3\text{-Fe}_2\text{O}_3$  nanotubes are shown in Fig. 2 to further investigate the nanostructures. The TEM images indicate that both samples possess nanotube structures. The average grain sizes are about 35 nm for pure  $\text{Fe}_2\text{O}_3$  and 7 nm for 3 wt%  $\text{Er}_2\text{O}_3\text{-Fe}_2\text{O}_3$ . The grain size becomes much smaller after doping Er. The typical XRD patterns of pure  $\alpha\text{-Fe}_2\text{O}_3$  and 3 wt%  $\text{Er}_2\text{O}_3\text{-Fe}_2\text{O}_3$  nanotubes calcined at 550 °C are displayed in Fig. 3. All the diffraction peaks of pure  $\alpha\text{-Fe}_2\text{O}_3$  nanotubes are well matched to hematite (JCPDS: 79-1741). No other peaks are observed. The peaks changed slightly and a weak peak of  $\text{Er}_2\text{O}_3$  is observed due to the small amount of dopant. The main peaks can be indexed to the hexagonal crystal  $\text{Fe}_2\text{O}_3$ . The lattice constants are  $a = 5.034 \text{ \AA}$  and  $c = 13.746 \text{ \AA}$ . Debye-Scherrer formula

$$D = \frac{K\lambda}{\beta \cos(\theta)},$$

is introduced to calculate the grain size according to the peaks (110) and (214), where  $D$  is the grain size,  $K$  is a constant (0.89),  $\lambda$  is the x-ray wavelength (0.15406 nm), and  $\beta$  is the full width at half-maximum of the  $2\theta$  diffraction peak. The average grain sizes are about 36.7 nm for pure  $\alpha\text{-Fe}_2\text{O}_3$  and 9.1 nm for 3 wt%  $\text{Er}_2\text{O}_3\text{-Fe}_2\text{O}_3$ , respectively. These values well matched the results of TEM. As we know, the smaller grain size is beneficial to the gas sensing properties of materials.<sup>[17]</sup>

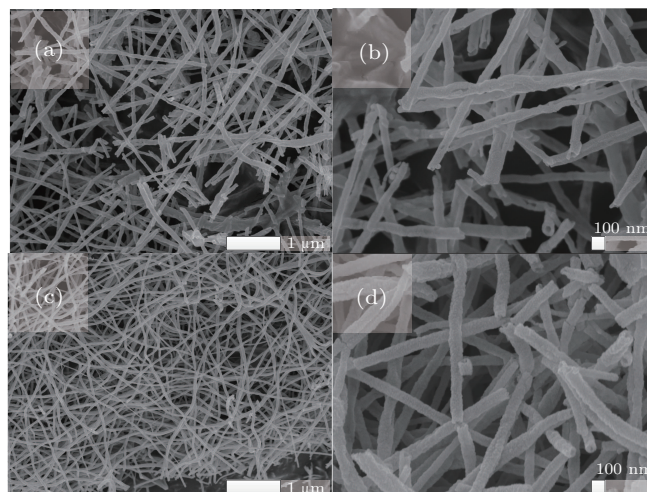


Fig. 1. SEM images of pure  $\alpha\text{-Fe}_2\text{O}_3$  ((a) and (b)) and 3 wt%  $\text{Er}_2\text{O}_3\text{-Fe}_2\text{O}_3$  nanotubes ((c) and (d)).

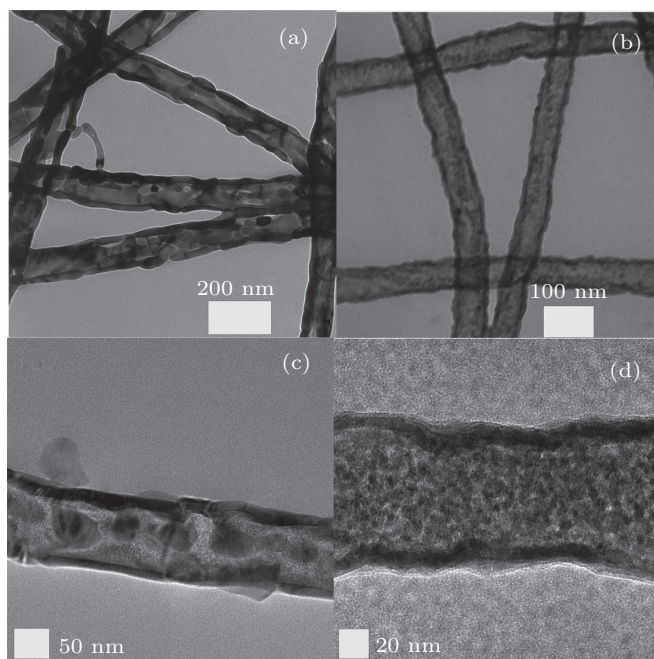


Fig. 2. TEM images of pure  $\alpha$ -Fe<sub>2</sub>O<sub>3</sub> nanotubes ((a) and (c)) and 3 wt% Er<sub>2</sub>O<sub>3</sub>-Fe<sub>2</sub>O<sub>3</sub> nanotubes ((b) and (d)).

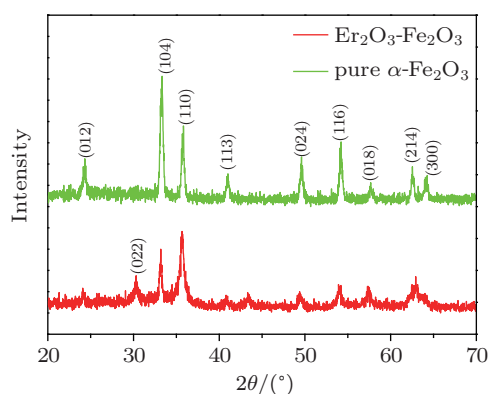


Fig. 3. (color online) XRD patterns of pure  $\alpha$ -Fe<sub>2</sub>O<sub>3</sub> and 3 wt% Er<sub>2</sub>O<sub>3</sub>-Fe<sub>2</sub>O<sub>3</sub> nanotubes calcined at 550 °C.

### 3.2. Discussion of sensing properties of materials

Pure, 1 wt%, 3 wt%, and 5 wt% Er-doped  $\alpha$ -Fe<sub>2</sub>O<sub>3</sub> nanotube sensors were tested at different operating temperatures to 10 ppm ethanol and the results are shown in Fig. 4. It can be seen that all the response curves have the same tendency. Firstly, the responses of pure, 1 wt%, 3 wt%, and 5 wt% Er-doped  $\alpha$ -Fe<sub>2</sub>O<sub>3</sub> nanotube sensors increase with the operating temperature increasing and reach the maximum value at the operating temperature 240 °C. Then, the responses decrease rapidly with the operating temperature further increasing. Thus, 240 °C is chosen as the optimum operating temperature. This performance can be explained as follows. The reaction rate between adsorbed oxygen species and ethanol is low at a low operating temperature. When the operating temperature reaches the optimum value, the adsorption and desorption rates of ethanol and oxygen species achieve a balance, and the response reaches a maximum value. With the

operating temperature further increasing, the desorption performance is stronger than the adsorption, this results in the response decreasing.<sup>[34,35]</sup> The 1 wt%, 3 wt%, and 5 wt% Er-doped  $\alpha$ -Fe<sub>2</sub>O<sub>3</sub> nanotube sensors show improved sensitivities to ethanol than pure  $\alpha$ -Fe<sub>2</sub>O<sub>3</sub> nanotube sensors. The response values are about 1.5, 7.6, 21, and 12.5 of 0 wt%, 1 wt%, 3 wt%, and 5 wt% Er-doped  $\alpha$ -Fe<sub>2</sub>O<sub>3</sub> nanotube sensors at 240 °C, respectively. Moreover, 3 wt% Er-doped  $\alpha$ -Fe<sub>2</sub>O<sub>3</sub> nanotube sensors show the best sensitivity to 10 ppm ethanol. The response value reaches 21 at 240 °C, which is much higher than that of pure  $\alpha$ -Fe<sub>2</sub>O<sub>3</sub> nanotube sensors. Namely, the ethanol sensitivity of pure  $\alpha$ -Fe<sub>2</sub>O<sub>3</sub> nanotubes is enhanced remarkably by doping Er. The 3 wt% Er-doped  $\alpha$ -Fe<sub>2</sub>O<sub>3</sub> nanotubes material is chosen for further research and written as Er<sub>2</sub>O<sub>3</sub>-Fe<sub>2</sub>O<sub>3</sub>.

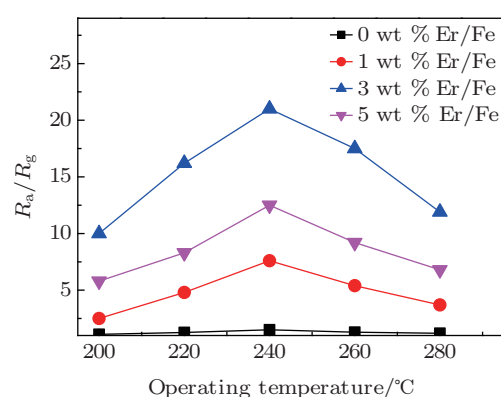


Fig. 4. (color online) Response curves of pure, 1 wt%, 3 wt%, and 5 wt% Er-doped  $\alpha$ -Fe<sub>2</sub>O<sub>3</sub> nanotube sensors at different operating temperatures to 10 ppm ethanol.

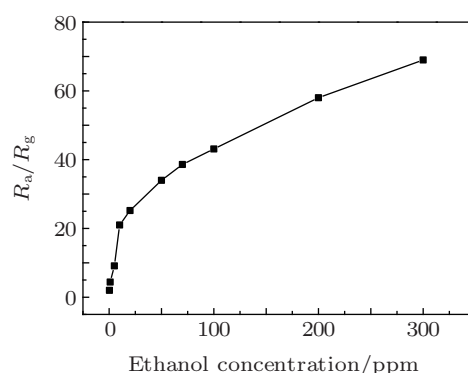


Fig. 5. The response curve of Er<sub>2</sub>O<sub>3</sub>-Fe<sub>2</sub>O<sub>3</sub> nanotube sensors at different ethanol concentrations at 240 °C.

Er<sub>2</sub>O<sub>3</sub>-Fe<sub>2</sub>O<sub>3</sub> nanotube sensors were tested at different ethanol concentrations at 240 °C, and the results are displayed in Fig. 5. The response curve shows that the response increases rapidly at the low ethanol concentration. Then the response increases tardily with the ethanol concentration further increasing. One of the most important factors to gas sensors is the lowest detection limit. The lowest detection limit of Er<sub>2</sub>O<sub>3</sub>-Fe<sub>2</sub>O<sub>3</sub> nanotube sensors is 300 ppb ethanol, to which

the response value is about 2. It means that  $\text{Er}_2\text{O}_3\text{-Fe}_2\text{O}_3$  nanotube sensors could detect a small amount of ethanol, which is crucial in practical application. In addition, the  $\text{Er}_2\text{O}_3\text{-Fe}_2\text{O}_3$  nanotube sensors show a wonderful sensitive to ethanol.

Table 1 indicates that  $\text{Er}_2\text{O}_3\text{-Fe}_2\text{O}_3$  nanotube sensors show a better sensitivity to ethanol than other ethanol sensors based on other  $\text{Fe}_2\text{O}_3$  materials. Hence, the  $\text{Er}_2\text{O}_3\text{-Fe}_2\text{O}_3$  nanotubes have potential to be used for ethanol sensors.

**Table 1.** Comparison between sensors based on  $\text{Er}_2\text{O}_3\text{-Fe}_2\text{O}_3$  nanotubes and other ethanol gas sensors of  $\text{Fe}_2\text{O}_3$ .

Gas sensor	Definition of sensitivity	Operating temperature/ $^{\circ}\text{C}$	Ethanol concentration/ppm	Value of sensitivity	Reference
$\text{Er}_2\text{O}_3\text{-Fe}_2\text{O}_3$	$R_a/R_g$	240	10	21	this work
$\text{In}_2\text{O}_3/\alpha\text{-Fe}_2\text{O}_3$	$R_a/R_g$	225	100	21.4	[36]
Cu-doped $\alpha\text{-Fe}_2\text{O}_3$	$R_a/R_g$	225	100	19.2	[23]
$\text{Fe}_2\text{O}_3\text{-G}$	$R_a/R_g$	280	1000	30	[14]
Core-shell $\text{SnO}_2/\alpha\text{-Fe}_2\text{O}_3$	$R_a/R_g$	340	100	22	[37]
$\text{SnO}_2/\alpha\text{-Fe}_2\text{O}_3$ nanotubes	$R_a/R_g$	200	100	28	[20]

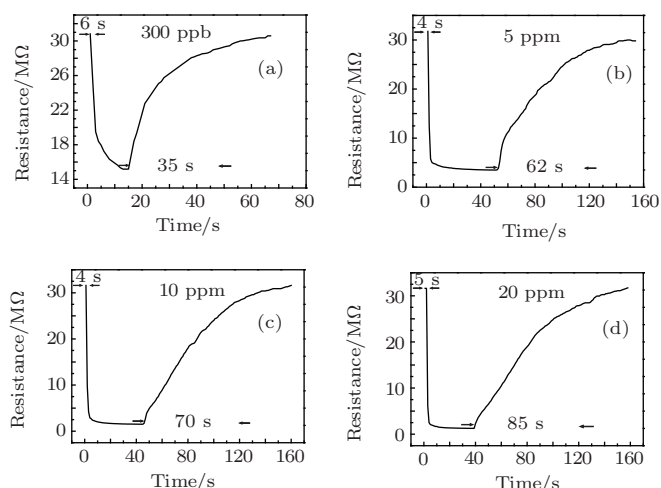


**Fig. 6.** The response and recovery curves of  $\text{Er}_2\text{O}_3\text{-Fe}_2\text{O}_3$  nanotube sensors to 300 ppb (a), 5 ppm (b), 10 ppm (c), and 20 ppm (d) ethanol at  $240^{\circ}\text{C}$ .

$\text{Er}_2\text{O}_3\text{-Fe}_2\text{O}_3$  nanotube sensors have been tested to ethanol and some other common gases, and the results are shown in Fig. 7. It can be seen that  $\text{Er}_2\text{O}_3\text{-Fe}_2\text{O}_3$  nanotube sensors show a wonderful sensitive property to ethanol, and the response values are about 9.1 and 21 to 5 ppm and 10 ppm ethanol, respectively. However, the  $\text{Er}_2\text{O}_3\text{-Fe}_2\text{O}_3$  nanotube sensors show less sensibility to other common sensitive gases. These indicate that the  $\text{Er}_2\text{O}_3\text{-Fe}_2\text{O}_3$  nanotube sensors possess a good selectivity, which makes  $\text{Er}_2\text{O}_3\text{-Fe}_2\text{O}_3$  nanotubes to be used for ethanol sensors. The response values to different gases are different, which may be due to the characteristics of materials. The previous work has explained that the same sensor could detect different gases by setting different operating temperatures. The energies of different gases for adsorption, desorption, and reaction on the material are different. Hence, the sensitivities of the sensors to different gases at

The response and recovery curves of  $\text{Er}_2\text{O}_3\text{-Fe}_2\text{O}_3$  nanotube sensors to 300 ppb, 5 ppm, 10 ppm, and 20 ppm ethanol at  $240^{\circ}\text{C}$  are shown in Fig. 6. It can be seen that the four curves display the same tendency. The response time is about 6 s, 4 s, 4 s, and 5 s to 300 ppb, 5 ppm, 10 ppm, and 20 ppm ethanol, respectively. The  $\text{Er}_2\text{O}_3\text{-Fe}_2\text{O}_3$  nanotube sensors show a fast response. However, the recovery time is about 35 s, 62 s, 70 s, and 85 s, respectively.

the same temperature are different, which depends on the gas being sensed and the characteristics of the materials. [38,39]

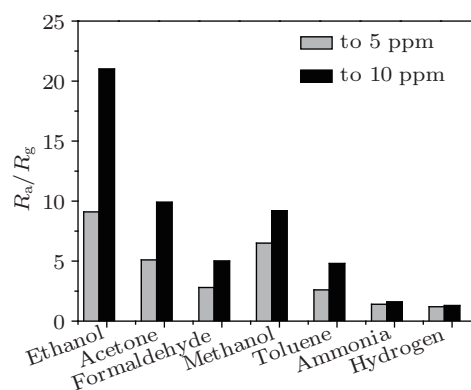


**Fig. 7.** The responses of  $\text{Er}_2\text{O}_3\text{-Fe}_2\text{O}_3$  nanotube sensors to different gases at  $240^{\circ}\text{C}$ .

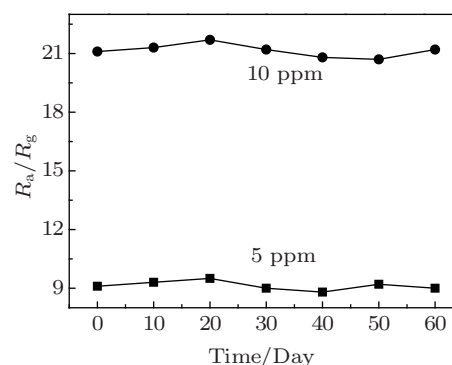


**Fig. 8.** Responses of  $\text{Er}_2\text{O}_3\text{-Fe}_2\text{O}_3$  nanotube sensors to 5 and 10 ppm ethanol every ten days at  $240^{\circ}\text{C}$ .

The  $\text{Er}_2\text{O}_3\text{-Fe}_2\text{O}_3$  nanotube sensors were tested to 5 and 10 ppm ethanol every ten days at  $240^{\circ}\text{C}$  and the results are

shown in Fig. 8. It can be seen that the ethanol sensing property of  $\text{Er}_2\text{O}_3\text{-Fe}_2\text{O}_3$  nanotube sensors possess a good long-term stability, due to the stability of  $\text{Fe}_2\text{O}_3$ . This characteristic indicates that  $\text{Er}_2\text{O}_3\text{-Fe}_2\text{O}_3$  nanotubes could be applied in practical application.

### 3.3. Sensing mechanism

The  $\alpha\text{-Fe}_2\text{O}_3$  is an n-type semiconductor, the sensing mechanism can be explained as follows. The response is caused by the change of the sensor resistance. As we know, when the sensor is exposed to the air, the  $\text{O}_2$  will be adsorbed on the surface of  $\text{Fe}_2\text{O}_3$ , then the  $\text{O}_2$  will catch electrons from the semiconductor oxides and turn to  $\text{O}_2^-$ ,  $\text{O}^-$ , and  $\text{O}^{2-}$ . A wide electron depleted layer will form on the material surface and increase the barrier height for electrons to transport. As a result, the conductivity of  $\text{Fe}_2\text{O}_3$  declines. When the sensor is exposed to a target gas, like ethanol, ethanol will react with oxygen species ( $\text{O}_2^-$ ,  $\text{O}^-$ , and  $\text{O}^{2-}$ ) and form  $\text{CO}_2$  and  $\text{H}_2\text{O}$ . The electron-depleted layer decreases, and the electron is released to improve the conductivity of  $\text{Fe}_2\text{O}_3$  at the same time.<sup>[40,41]</sup> Thus the resistance change of  $\text{Fe}_2\text{O}_3$  is formed.<sup>[42]</sup> As the formulas describe

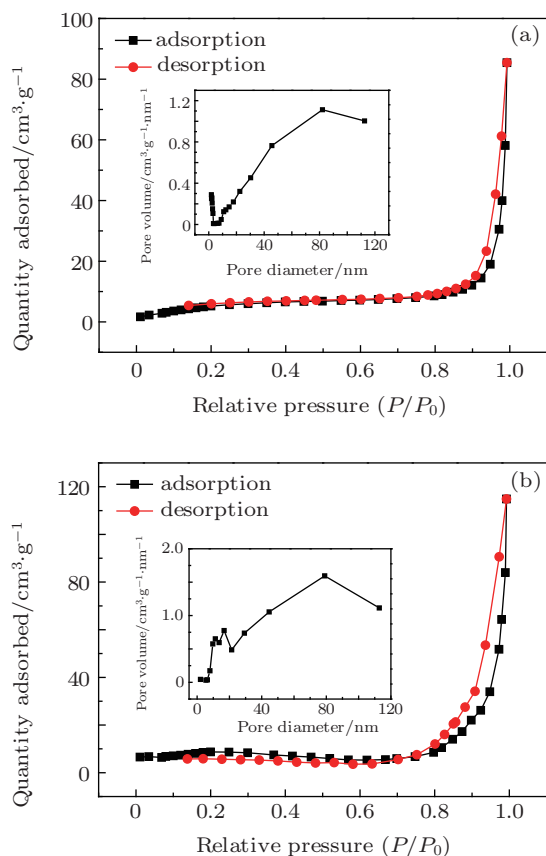
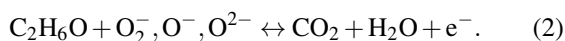
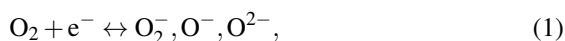


**Fig. 9.** (color online) The  $\text{N}_2$  adsorption-desorption isotherm and BJH pore size distribution curves (inset) of pure  $\alpha\text{-Fe}_2\text{O}_3$  nanotubes (a) and  $\text{Er}_2\text{O}_3\text{-Fe}_2\text{O}_3$  nanotubes (b) at standard temperature and pressure.

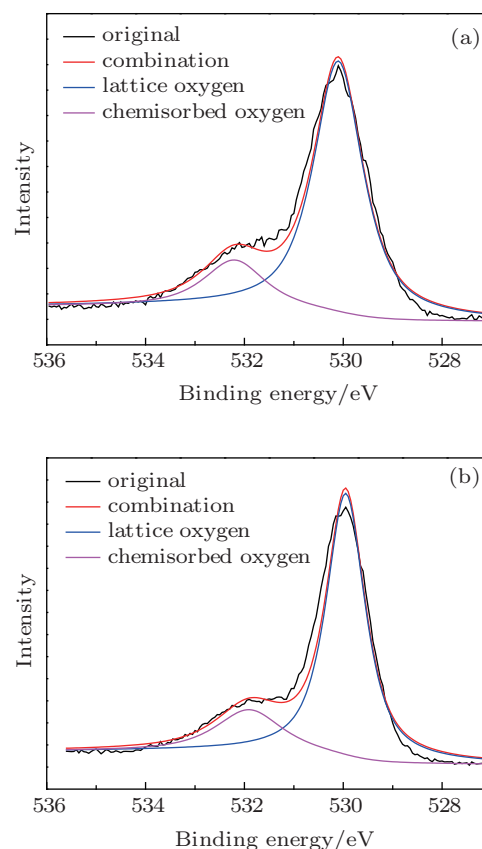


**Fig. 10.** (color online) The XPS spectra of O1s of pure  $\alpha\text{-Fe}_2\text{O}_3$  nanotubes (a) and  $\text{Er}_2\text{O}_3\text{-Fe}_2\text{O}_3$  nanotubes (b).

$\text{N}_2$  adsorption-desorption isotherm and BJH pore size distribution curves (inset of Fig. 9(a)) of pure  $\alpha\text{-Fe}_2\text{O}_3$  nanotubes and  $\text{Er}_2\text{O}_3\text{-Fe}_2\text{O}_3$  nanotubes are shown in Figs. 9(a) and 9(b). The BET surface area of pure  $\alpha\text{-Fe}_2\text{O}_3$  nanotubes and  $\text{Er}_2\text{O}_3\text{-Fe}_2\text{O}_3$  nanotubes are 22.1 and 27.9  $\text{m}^2/\text{g}$ , respectively, which are relatively higher BET surface areas.<sup>[21,43]</sup> Moreover, BET surface area of  $\text{Er}_2\text{O}_3\text{-Fe}_2\text{O}_3$  nanotubes is higher than that of pure  $\alpha\text{-Fe}_2\text{O}_3$  nanotubes. The higher BET surface area will lead to a higher sensitivity. The nanotube structure is an open and high surface-to-volume ratio nanostructure, which will provide large sites for adsorption, desorption, and reaction, not only the outer surface of the material, but also the exposure of the inner surface. This is beneficial to the gas sensing property.<sup>[21,22]</sup> XPS spectra of O1s of pure  $\alpha\text{-Fe}_2\text{O}_3$  nanotubes and  $\text{Er}_2\text{O}_3\text{-Fe}_2\text{O}_3$  nanotubes are displayed in Figs. 10(a) and 10(b). The chemisorbed oxygen contents of pure  $\alpha\text{-Fe}_2\text{O}_3$  nanotubes and  $\text{Er}_2\text{O}_3\text{-Fe}_2\text{O}_3$  nanotubes are about 19% and 24%, respectively.  $\text{Er}_2\text{O}_3\text{-Fe}_2\text{O}_3$  nanotubes will chemisorb more oxygen than pure  $\alpha\text{-Fe}_2\text{O}_3$  nanotubes due to the more defects which are resulted from the doping of Er. On the one hand, the enhanced ethanol sensing property of  $\text{Er}_2\text{O}_3\text{-Fe}_2\text{O}_3$  nanotubes is attributed to Er-dopant which will lead to more defects and vacancies, which means that more oxygen will be chemisorbed on the  $\text{Er}_2\text{O}_3\text{-Fe}_2\text{O}_3$  nanotubes surface. Then, the more chemisorbed oxygen species will react with ethanol, that will result in a more violent reac-

tion and a higher response. Thus, the enhanced ethanol sensing property of  $\text{Er}_2\text{O}_3\text{-Fe}_2\text{O}_3$  nanotubes is caused by the increased defects and vacancies due to the Er-dopant.<sup>[31,32]</sup> On the other hand, the grain size of  $\text{Er}_2\text{O}_3\text{-Fe}_2\text{O}_3$  is much smaller than that of pure  $\alpha\text{-Fe}_2\text{O}_3$  due to the doping. As we know, the small grain size is beneficial to the gas sensing properties of materials.<sup>[17]</sup>

#### 4. Conclusion

In summary, pure  $\alpha\text{-Fe}_2\text{O}_3$  and  $\text{Er}_2\text{O}_3\text{-Fe}_2\text{O}_3$  nanotubes are successfully prepared via electrospinning method. The research of the gas sensing properties has indicated that doping Er is a wonderful way to enhance the ethanol sensing properties of  $\alpha\text{-Fe}_2\text{O}_3$  nanotubes.  $\text{Er}_2\text{O}_3\text{-Fe}_2\text{O}_3$  nanotubes show a wonderful sensitivity to ethanol at low concentrations. The response value is 21 to 10 ppm ethanol at the optimum operating temperature of 240 °C. Moreover, the  $\text{Er}_2\text{O}_3\text{-Fe}_2\text{O}_3$  nanotubes display a fast response time, good selectivity, and long-term stability. These advantages mean  $\text{Er}_2\text{O}_3\text{-Fe}_2\text{O}_3$  nanotubes can be used for gas sensors.

#### References

- [1] Brandt A and Balducci A 2013 *J. Power Sources* **230** 44
- [2] Xiao Y, Hu C and Cao M 2014 *J. Power Sources* **247** 49
- [3] Kar P, Banerjee T, Verma S, Sen A, Das A, Ganguly B and Ghosh H N 2012 *Phys. Chem. Chem. Phys.* **14** 8192
- [4] Leschkie K S, Divakar R, Basu J, Enache-Pommer E, Boecker J E, Carter C B, Kortshagen U R, Norris D J and Aydil E S 2007 *Nano Lett.* **7** 1793
- [5] Katoch A, Byun J H, Choi S W and Kim S S 2014 *Sens. Actuators B* **202** 38
- [6] Zeng P, Zhang P, Hu M, Ma S Y and Yan W J 2014 *Chin. Phys. B* **23** 058103
- [7] Qin Y X, Liu C Y and Liu Y 2015 *Chin. Phys. B* **24** 027304
- [8] Jabben M, Iqbal M A, Kumar R V, Ahmed M and Javed M T 2014 *Chin. Phys. B* **23** 018504
- [9] Michel C R and Martínez-Preciado A H 2015 *Sens. Actuators B* **208** 355
- [10] Zeng W, Li T, Li T, Hao J and Li Y 2015 *J. Mater. Sci.-Mater. Electron.* **26** 1192
- [11] Zhang Y, Liu T, Zhang H, Zeng W, Pan F and Peng X 2014 *J. Mater. Sci.-Mater. Electron.* **26** 191
- [12] Sun G, Qi F, Zhang S, Li Y, Wang Y, Cao J, Bala H, Wang X, Jia T and Zhang Z 2014 *J. Alloy. Compd.* **617** 192
- [13] Song P, Han D, Zhang H, Li J, Yang Z and Wang Q 2014 *Sens. Actuators B* **196** 434
- [14] Liang S, Zhu J, Wang C, Yu S, Bi H, Liu X and Wang X 2014 *Appl. Sur. Sci.* **292** 278
- [15] Zhao C, Huang B, Xie E, Zhou J and Zhang Z 2015 *Sens. Actuators B* **207** 313
- [16] Jiang Z, Jiang T, Wang J, Wang Z, Xu X, Wang Z, Zhao R, Li Z and Wang C 2015 *J. Colloid. Interface. Sci.* **437** 252
- [17] Sun X, Ji H, Li X, Cai S and Zheng C 2014 *J. Alloy. Compd.* **600** 111
- [18] Fan H, Zhang T, Xu X and Lv N 2011 *Sens. Actuators B* **153** 83
- [19] Peeters D, Barreca D, Carraro G, Comini E, Gasparotto A, Maccato C, Sada C and Sberveglieri G 2014 *J. Phys. Chem. C* **118** 11813
- [20] Zhao C, Hu W, Zhang Z, Zhou J, Pan X and Xie E 2014 *Sens. Actuators B* **195** 486
- [21] Liu C, Chi X, Liu X and Wang S 2014 *J. Alloy. Compd.* **616** 208
- [22] Du N, Zhang H, Chen B D, Ma X Y, Liu Z H, Wu J B and Yang D R 2007 *Adv. Mater.* **19** 1641
- [23] Sun P, Wang C, Zhou X, Cheng P, Shimanoe K, Lu G and Yamazoe N 2014 *Sens. Actuators B* **193** 616
- [24] Gunawan P, Mei L, Teo J, Ma J, Highfield J, Li Q and Zhong Z 2012 *Langmuir* **28** 14090
- [25] Xu L, Dong B, Wang Y, Bai X, Chen J, Liu Q and Song H 2010 *J. Phys. Chem. C* **114** 9089
- [26] Aono H, Traversa E, Sakamoto M and Sadaoka Y 2003 *Sens. Actuators B* **94** 132
- [27] Wang C, Ma S, Sun A, Qin R, Yang F, Li X, Li F and Yang X 2014 *Sens. Actuators B* **193** 326
- [28] Rajgure A V, Tarwal N L, Patil J Y, Chikhale L P, Pawar R C, Lee C S, Mulla I S and Suryavanshi S S 2014 *Ceram. Int.* **40** 5837
- [29] Su C, Liu C, Liu L, Ni M, Li H, Bo X, Liu L and Chi X 2014 *Appl. Surf. Sci.* **314** 931
- [30] Li W, Ma S, Yang G, Mao Y, Luo J, Cheng L, Gengzang D, Xu X and Yan S 2015 *Mater. Lett.* **138** 188
- [31] Zhang T, Gu F, Han D, Wang Z and Guo G 2013 *Sens. Actuators B* **177** 1180
- [32] Zhang X H, Chen J, Wu Y, Xie Z, Kang J and Zheng L 2011 *Colloid. Surface. A* **384** 580
- [33] Liu L, Liu C, Li S, Wang L, Shan H, Zhang X, Guan H and Liu Z 2013 *Sens. Actuators B* **177** 893
- [34] Mao Y, Ma S, Li X, Wang C, Li F, Yang X, Zhu J and Ma L 2014 *Appl. Surf. Sci.* **298** 109
- [35] Hjiri M, El Mir L, Leonardi S G, Pistone A, Mavilia L and Neri G 2014 *Sens. Actuators B* **196** 413
- [36] Zhao C, Zhang G, Han W, Fu J, He Y, Zhang Z and Xie E 2013 *Cryst. Eng. Commun.* **15** 6491
- [37] Wang B B, Fu X X, Liu F, Shi S L, Cheng J P and Zhang X B 2014 *J. Alloy. Compd.* **587** 82
- [38] Navale S T, Bandgar D K, Nalage S R, Khuspe G D, Chougule M A, Kolekar Y D, Sen S and Patil V B 2013 *Ceram. Int.* **39** 6453
- [39] Zheng W, Li Z, Zhang H, Wang W, Wang Y and Wang C 2009 *Mater. Res. Bull.* **44** 1432
- [40] Lou Z, Li F, Deng J, Wang L and Zhang T 2013 *ACS Appl. Mater. Inter.* **5** 12310
- [41] Li X B, Ma S Y, Li F M, Chen Y, Zhang Q Q, Yang X H, Wang C Y and Zhu J 2013 *Mater. Lett.* **100** 119
- [42] Ma J, Teo J, Mei L, Zhong Z, Li Q, Wang T, Duan X, Lian J and Zheng W 2012 *J. Mater. Chem.* **22** 11694
- [43] Li W Q, Ma S Y, Li Y F, Li X B, Wang C Y, Yang X H, Cheng L, Mao Y Z, Luo J, Gengzang D J, Wan G X and Xu X L 2014 *J. Alloy. Compd.* **605** 80